Dynamic Range by Design in OTA EVM measurements

Paritosh Manurkar[1,2], Daniel G. Kuester[2], Joshua M. Kast[2,3], Robert D. Horansky[2]

[1]University of Colorado, Boulder, USA, [2]National Institute of Standards and Technology, Boulder, USA, [3]Colorado School of Mines, Golden, USA

***Abstract* — We present an experimental approach to design an over-the-air (OTA) millimeter-wave system for measuring error vector magnitude (EVM) with associated uncertainties that include correlations and nonlinearities. Our approach uses a variable waveguide attenuator at the output of a modulated-signal source at 44 GHz and provides traceable measurements on a calibrated equivalent-time sampling oscilloscope. The conductor-based EVM measurements and associated uncertainties presented here serve as a baseline for the eventual OTA-based EVM. We also discuss a noise based EVM estimation technique as a simple tool for planning OTA EVM measurements, but without a complete knowledge of measurement uncertainties.**

***Index Terms* — Digitally modulated signals, error vector magnitude, Over-the-air measurements, uncertainty analysis, wireless system.**

I. Introduction

Over-the-air (OTA) measurements are key for testing at millimeter-wave frequencies since using cables is often not feasible [1]. A commonly-used metric for evaluating OTA performance at the system or device level is error vector magnitude (EVM) [2]–[5]. Our previous publications have detailed the role modulated-signal sources can play in calibrating receivers in the laboratory setting [6], [7]. Although these demonstrations were in the conducted medium, such sources can also be used for OTA measurements at millimeter-wave frequencies to calibrate other instruments.

An extension of the recently published IEEE 1765-2022 Recommended Practice for EVM Measurement and Uncertainty Evaluation makes use of modulated-signal sources for OTA measurements. The IEEE 1765-2022 recommended practice [8], [9] demonstrates how users can study the impact their receiver has on the measurement of EVM, along with its associated uncertainty. This is done by comparing their measurements with those performed on a reference receiver calibrated at a reference lab such as a National Metrology Institute (NMI). The independently calibrated reference receiver characterizes the EVM of the modulated-signal source. Keeping the rest of the measurement setup unchanged and only replacing the reference receiver with a user receiver, the impact of the user receiver on the EVM and associated uncertainty can be compared with that of the reference receiver [10]. To obtain EVM distributions for OTA measurements similar to those in the conducted case and to optimally utilize the available resources, most importantly, equipment and time, we first need to develop methodologies to optimize OTA measurements for this application, test them, and then implement them in the laboratory setting.

In this paper, we present an experimental approach in the conducted setting to design an OTA experiment with focus on the measured EVM and associated uncertainties. We also provide a comparison with EVM estimates based on a noise-based technique. The knowledge we can gain from the experimental approach and the noise-based technique is two-fold. Given the expected path loss based on the separation between TX and RX horn antennas in our OTA experiment, our approach provides baseline curves to expect in the eventual OTA measurement for both the measured EVM and the uncertainty in EVM, whereas the noise-based technique provides an approximate EVM value based only on measured traces. The methods discussed in this paper can be useful and less time-consuming depending on the specific requirements during the planning stages of an OTA experiment.

II. Approach

Our experimental approach uses a waveguide variable attenuator—referred to as the channel attenuator—to mimic the OTA path and provide an OTA baseline EVM curve along with associated uncertainties. In other words, given the path losses we would expect to encounter in an OTA measurement, we can a priori estimate the EVM and associated uncertainty in our measurement to provide the highest dynamic range OTA measurements as possible. This approach can be useful in designing an OTA experiment where, for instance, the separation between the TX and RX antennas is swept to study the resulting EVM values and associated uncertainties. It can help maximize the dynamic range of the OTA system with a focus on increasing repeatability of the system. We define the EVM dynamic range for this discussion as the ratio, expressed in dB, of the highest reasonable EVM after channel attenuation to the EVM of the predistorted signal measured before inserting the channel attenuator.

Additionally, we show that we can employ the signal-to-noise-and-distortion (SINAD) ratio for a rough estimate to design an OTA experiment using the inverse square root dependence of EVM [11]–[13]. It should be noted that the SINAD approximation is limited to EVM caused by Gaussian noise and distortion, and thus it cannot replace the elaborate measurement, postprocessing, and uncertainty estimation presented here that provides the measurement uncertainties on top of the dynamic range of the measured EVM [6], [7], [14].

2023 101st ARFTG Microwave Measurement Conference (ARFTG) | 979-8-3503-2345-0/23/$31.00 ©2023 IEEE | DOI: 10.1109/ARFTG57476.2023.10278895

A. Experimental method

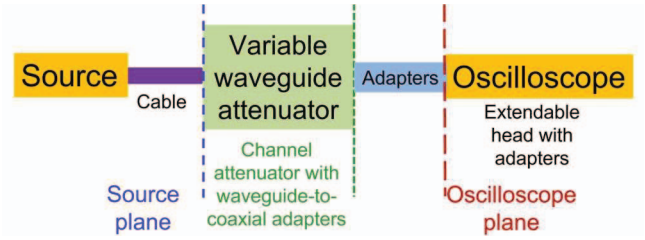

Fig. 1. Experimental schematic. Measurements are made on the oscilloscope first, without and then with the channel attenuator. The reference planes (dashed lines) play an important role for measuring correct EVM values.

We used a modulated-signal source (shown as "Source" in Fig. 1) at 44 GHz for this demonstration. As with our previous work, this source was also locked to a precise 10-GHz tone. The signal to be measured, which was the ideal reference waveform at 4 GHz from IEEE 1765-2022 [9] was uploaded on the arbitrary waveform generator (AWG). The 4-GHz signal was mixed with a frequency-quadrupled 10-GHz tone to produce the modulated signal at 44 GHz. This signal was first measured without the channel attenuator at the oscilloscope plane on an equivalent-time sampling oscilloscope (marked as "Oscilloscope" in Fig. 1), which has been calibrated in phase via a photodiode standard. The photodiode was traceably calibrated using the NIST electro-optic sampling (EOS) technique. The oscilloscope can also be calibrated in power using the NIST power sensor and is, therefore, capable of performing traceable measurements [15], [16].

We predistorted the signal iteratively based on the oscilloscope measurements without the channel attenuator in the setup to provide a near-ideal version of the designed signal at the source plane. In each iteration, the reference plane was transferred from the oscilloscope plane (red) to the source plane (blue). EVM was computed using the Baseline EVM Algorithm also developed in IEEE 1765-2022. We then measured eight repeats each consisting of 25 oscilloscope measurements of the last predistorted signal for estimating uncertainty at the source plane. Each reported value of EVM includes uncertainties resulting from the repeat oscilloscope measurements, the oscilloscope's residual timebase distortion, drift, and residual source- and oscilloscope mismatch, and oscilloscope internal response corrections [6], [7].

With the ideal signal predistorted to the source reference plane, the predistorted signal was uploaded to the AWG, the channel attenuator was inserted after the source plane and the output signal was measured on the equivalent-time sampling oscilloscope. We varied the channel attenuation from 0 dB to 50 dB to study the effect of the path loss on the measured EVM and its associated uncertainty. At each channel attenuation setting, we adjusted the voltage scale for the attenuated signal and repeated three sets each consisting of 25 oscilloscope measurements one after another to include data collection repeatability in the uncertainty estimation. For this postprocessing, the reference plane was transferred from the oscilloscope (red) plane to the channel attenuator (green) plane where we could ascertain the impact of the channel attenuator on the previously produced low-EVM signal.

B. Uncertainty Estimation

For uncertainty analyses, both without and with the channel attenuator, the oscilloscope measurements were corrected for the oscilloscope's timebase distortions, averaged, and drift corrected., The uncertainties associated with the source mismatch, the adapters between the source and the oscilloscope, the oscilloscope mismatch, and the oscilloscope response were propagated in the NIST Microwave Uncertainty Framework [17], which tracks correlated uncertainties while transferring the calibrated measurements at the oscilloscope plane to the source plane after de-embedding the adapters.

For the case with the channel attenuator, an updated source mismatch was utilized at the green reference plane. The VNA measurements for source mismatch and the channel attenuator, along with their computed uncertainties were cascaded in the NIST Microwave Uncertainty Framework to propagate the uncertainties to the green reference plane. Then, the calibrated measurements at the oscilloscope plane were also transferred to the green plane after de-embedding the adapters. For each attenuator setting, the uncertainty estimation yielded EVM distributions, Monte-Carlo mean EVMs, and 95% confidence limits, which were saved to plot the data shown in Fig. 3.

C. EVM approximation using noise-based technique

In addition to the conducted-channel attenuator measurement and uncertainty estimation procedures presented thus far, an easier way to obtain an approximate baseline EVM curve without uncertainties is an experiment based on SNR and SINAD calculations from measured traces. This noise-based technique assumes that the EVM is due to Gaussian-distributed noise and/or distortion. It can be useful for planning an OTA experiment when a complete uncertainty analysis—which requires additional measurements and resources—is too time consuming. However, the conducted experimental approach is recommended for a complete knowledge of the dynamic range in EVM and the associated uncertainties.

Fig. 2 shows example spectra that highlight various signal and background levels during the channel attenuator sweep measurements. The spectra are obtained after transforming the postprocessed oscilloscope time-domain data into frequency domain. The frequency axis is relative to the respective IF or RF center frequencies so that contributions from different equipment can be highlighted on the same plot. The total (blue) spectrum is centered at 44 GHz. The AWG contributes a raised noise floor due to AWG background noise/distortion which we refer to as the AWG pedestal. The pedestal spectrum (red) shown here is centered at ~45.8 GHz, beyond the signal bandwidth and is used to estimate the in-band AWG distortion. The oscilloscope (yellow) spectrum shows the background noise level of the equivalent-time sampling oscilloscope and is

centered at ~15 GHz, beyond the signal and AWG pedestal bandwidths. It represents the true receiver noise floor of the measurements.

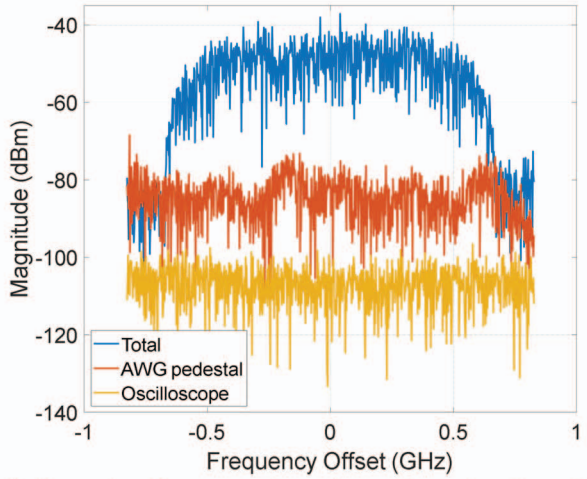

Fig. 2. Example of a measured spectrum shown together with its background noise and distortion from various instruments.

Based on the signal and background noise levels shown in Fig. 2, we can calculate the SNR and the SINAD ratio.

1) Signal-to-Noise Ratio

If P_{total} is the total signal power which includes the AWG pedestal and oscilloscope background contributions for the bandwidth shown in Fig. 2, P_{signal} is the signal power after subtracting the AWG and oscilloscope contributions and $P_{\text{n,scope}}$ is the oscilloscope background noise power for the same bandwidth, then we define SNR as follows:

$$\text{SNR} = \frac{P_{\text{signal}}}{P_{\text{n,scope}}}. \quad (1)$$

Here P_x is computed from the measured time-domain voltage $s(t)$ as $2\times\Sigma|S(f)|^2/50$, where x is either signal or n,scope, and $S(f)$ is the discrete Fourier transform computed using a numerical software package.

2) Signal-to-Noise-and-Distortion Ratio

For the spectra shown in Fig. 2, we again define P_{signal} as the signal power after subtracting the AWG and oscilloscope contributions, $P_{\text{AWGpedestal}}$ as the AWG pedestal power which includes the oscilloscope background. Then, we define SINAD as the ratio of signal to noise plus distortion,

$$\text{SINAD} = \frac{P_{\text{signal}}}{P_{\text{AWGpedestal}}}. \quad (2)$$

3) EVM estimation

We next estimate EVM based on SNR and SINAD using the square root approximation as follows

$$\text{EVM} \approx \frac{1}{\sqrt{\text{SNR}}} \text{ or } \frac{1}{\sqrt{\text{SINAD}}}. \quad (3)$$

III. Application to OTA Measurements

The Monte Carlo mean EVM, and the associated uncertainty (95% confidence limits plotted as error bars) at signal powers measured on the sampling oscilloscope corresponding to each channel attenuation level are shown in Fig. 3 as the red curve. The range of P_{signal} is -19.7 dBm to -75.3 dBm at channel attenuation from 0 dB to 50 dB.

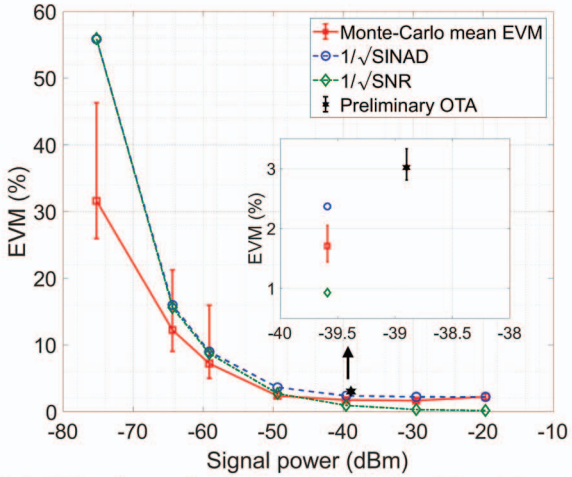

Fig. 3. EVM and associated uncertainty obtained from Monte Carlo simulation for measured signal powers corresponding to each channel attenuation along with the 95% confidence intervals as error bars. The plot also shows the EVM estimates from SNR (green diamonds) and SINAD (blue circles) formulations.

The EVM at signal power of -19.7 dBm is slightly higher than that at -29.6 dBm and -39.6 dBm of signal power. It was attributed to a high mismatch, and therefore, reflections between the oscilloscope module and the channel attenuator. We showed that a fixed 6-dB attenuator helps in improving the mismatch [18], but the data shown in Fig. 3 was measured before this demonstration. This curve provides the baseline EVM and uncertainty for the eventual OTA measurement using the modulated-signal source at 44 GHz. The EVM approximations from the coarse SNR and SINAD formulations discussed in II-C, are shown in Fig. 3 in green diamonds and blue circles, respectively. EVM estimates obtained using the coarse SINAD model are close enough to match the dynamic range of the EVM measurement for measured signal powers from -19.7 dBm to -64.4 dBm; and are slightly better at lower signal powers compared to the coarse SNR model because of the inclusion of AWG pedestal in the EVM calculation.

The fact that the measured EVM (red squares) and the estimates (green diamonds, blue circles) follow closely signifies that the estimates, primarily the EVM based on the SINAD formulation can be used as a parameter for OTA experiment design; however, in this case without the knowledge of measurement uncertainties.

Given that the predistorted signal at the source plane has a Monte-Carlo mean EVM of 1.4% and using the dynamic range definition from Section II, Fig. 3 shows that the OTA EVM measurements can be designed to provide a dynamic range of up to 7.1 dB with up to 7.2% Monte-Carlo mean EVM and 5$^{\text{th}}$ and 95$^{\text{th}}$ confidence limits of 5% and 15.9%, respectively, corresponding to the measured signal power of -59.1 dBm. For a lower measured signal, the EVM dynamic range is higher at 9.4 dB with up to 12.2% Monte-Carlo mean EVM at the cost of measurement uncertainty with 5$^{\text{th}}$ and 95$^{\text{th}}$ confidence limits of

9% and 21.2%, respectively. It should be noted that a higher dynamic range will only make sense for a measured signal that is still a faithful replica of the designed signal albeit with added noise and distortion.

Thus, we have the option to choose the dynamic range of measured EVM and associated uncertainties before performing an actual OTA experiment where, for instance, the separation between TX and RX horn antennas is varied for a fixed TX signal to study the impact on the measured EVM and the uncertainties. The measured EVM values in Fig. 3 give the EVM floor or baseline for such an OTA measurement resulting from various values of attenuation. Once more distortion and frequency dependent phase effects are added in an OTA transmission, we expect to see higher EVM than this baseline.

In a preliminary OTA experiment where TX and RX horn antennas were placed 1m apart, we measured an EVM of 3% with 5^{th} and 95^{th} confidence limits of 2.8% and 3.3%, respectively, at boresight. The corrected received signal power at the OTA RX reference plane was -38.9 dBm based on computed antenna gains of 23.35 dBm. From Fig. 3, we can see that the measured OTA EVM is slightly higher than the baseline as expected, and the preliminary OTA uncertainty estimation gives a 95% confidence interval (0.5%) that is close enough to that predicted by the attenuated measurement (0.6%).

IV. Conclusion

We have demonstrated that an attenuated sweep can aid in the design of an OTA measurement of EVM at a targeted baseline level of uncertainty at millimeter-wave frequencies using a precision modulated-signal source. Additionally, EVM estimation using SINAD can provide a heuristic technique to estimate the system's dynamic range. However, a thorough uncertainty propagation is required to provide a baseline for OTA-based measurements of EVM.

Acknowledgement

The authors would like to thank Kate A. Remley for her insights on modulated-signal source measurements and data processing, and Dylan F. Williams for fruitful discussions on the uncertainty analysis using the NIST Microwave Uncertainty Framework.

References

[1] M. Rumney, "Testing 5G: Time to throw away the cables," *Microw J*, pp. 10–18, Nov. 2016.

[2] M. E. Leinonen, N. Tervo, M. Jokinen, O. Kursu, and A. Pärssinen, "5G mmW Link Range Uncertainties From RF System Calculations and OTA Measurements," *IEEE Access*, vol. 9, pp. 31956–31966, 2021.

[3] D. Brown and Y. Rahmat-Samii, "Far Field EVM Characterization of Antenna Frequency Response via Full-Wave Analysis," in *2021 IEEE International Symposium on Antennas and Propagation and USNC-URSI Radio Science Meeting (APS/URSI)*, Dec. 2021, pp. 1251–1252.

[4] M. Löhning, T. Deckert, V. Kotzsch, and M. V. Bossche, "A Novel OTA Near-Field Measurement Approach Suitable for 5G mmWave Wideband Modulated Tests," in *2022 IEEE/MTT-S International Microwave Symposium - IMS 2022*, Jun. 2022, pp. 856–858.

[5] H. Chen, W. Lin, S. Wang, W. Che, and Q. Xue, "A Calibrated Over-the-Air Measurement Method for Error Vector Magnitude Characterization," *IEEE Trans. Instrum. Meas.*, vol. 71, pp. 1–8, 2022.

[6] K. A. Remley, D. F. Williams, P. D. Hale, C. Wang, J. Jargon, and Y. Park, "Millimeter-Wave Modulated-Signal and Error-Vector-Magnitude Measurement with Uncertainty," *IEEE Trans. Microw. Theory Tech.*, vol. 63, no. 5, pp. 1710–1720, May 2015.

[7] P. Manurkar, R. D. Horansky, B. F. Jamroz, J. A. Jargon, D. F. Williams, and K. A. Remley, "Precision Millimeter-Wave-Modulated Wideband Source at 92.4 GHz as a Step Toward an Over-the-Air Reference," *IEEE Trans. Microw. Theory Tech.*, vol. 68, no. 7, pp. 2644–2654, Jul. 2020.

[8] "IEEE SA - IEEE 1765-2022," *IEEE Standards Association*. https://standards.ieee.org/ieee/1765/10560/ (accessed Sep. 06, 2022).

[9] "Open-Source Repository: IEEE P1765 Recommended Practice for EVM Measurement and Uncertainty Evaluation," *GitLab*. https://opensource.ieee.org/1765/1765 (accessed Dec. 03, 2021).

[10] P. Manurkar, C. P. Silva, J. Kast, R. D. Horansky, D. F. Williams, and K. A. Remley, "Reference Measurements of Error Vector Magnitude," in *2022 IEEE/MTT-S International Microwave Symposium - IMS 2022*, Jun. 2022, pp. 1026–1029.

[11] H. A. Mahmoud and H. Arslan, "Error vector magnitude to SNR conversion for nondata-aided receivers," *IEEE Trans. Wirel. Commun.*, vol. 8, no. 5, pp. 2694–2704, May 2009.

[12] D. A. Humphreys and R. T. Dickerson, "Traceable measurement of Error Vector Magnitude (EVM) in WCDMA signals," in *2007 International Waveform Diversity and Design Conference*, Jun. 2007, pp. 270–274.

[13] D. A. Humphreys and J. Miall, "Traceable Measurement of Source and Receiver EVM Using a Real-Time Oscilloscope," *IEEE Trans. Instrum. Meas.*, vol. 62, no. 6, pp. 1413–1416, Jun. 2013.

[14] R. D. Horansky *et al.*, "Comparison of timebase interpolation methods for traceable, wideband mm-wave communication signals," in *2016 87th ARFTG Microwave Measurement Conference (ARFTG)*, May 2016, pp. 1–4.

[15] T. S. Clement, P. D. Hale, D. F. Williams, C. M. Wang, A. Dienstfrey, and D. A. Keenan, "Calibration of sampling oscilloscopes with high-speed photodiodes," *IEEE Trans. Microw. Theory Tech.*, vol. 54, no. 8, pp. 3173–3181, Aug. 2006.

[16] A. Dienstfrey, P. D. Hale, D. A. Keenan, T. S. Clement, and D. F. Williams, "Minimum-phase calibration of sampling oscilloscopes," *IEEE Trans. Microw. Theory Tech.*, vol. 54, no. 8, pp. 3197–3208, Aug. 2006.

[17] D. F. Williams and A. Lewandowski, "NIST Microwave Uncertainty Framework," *NIST*. 2011. [Online]. Available: http://www.nist.gov/ctl/rf-technology/related-software.cfm

[18] Manurkar, Paritosh, Kast, Joshua M., Williams, Dylan F., Horansky, Robert D., Kuester, Daniel G., and Remley, Kate A., "Recommended Practices for Calibrated Millimeter-Wave Modulated-Signal Measurements," in *2023 100th ARFTG Microwave Measurement Conference (ARFTG)*, Jan. 2023.